Investigation of the binding of *cis*/*trans*-[MCl₄(1*H*-indazole)(NO)]⁻ (M = Ru, Os) complexes to human serum albumin

Orsolya Dömötör[a,b], Anna Rathgeb[c], Paul-Steffen Kuhn[c], Ana Popović-Bijelić[d,*], Goran Bačić[d], Eva Anna Enyedy[a,*], Vladimir B. Arion[c,*]

[a]*Department of Inorganic and Analytical Chemistry, University of Szeged, Dóm tér 7, H-6720 Szeged, Hungary*

[b]*MTA-SZTE Bioinorganic Chemistry Research Group, University of Szeged, Dóm tér 7, H-6720 Szeged, Hungary*

[c]*University of Vienna, Institute of Inorganic Chemistry, Währinger Strasse 42, A-1090 Vienna, Austria*

[d]*EPR laboratory, Faculty of Physical Chemistry, University of Belgrade, Studentski trg 12-16, 11158 Belgrade, Serbia*

Keywords: Nitrosyl; Antitumor activity; Albumin binding; Fluorometry; EPR spin labeling

ABSTRACT

Overall binding affinity of sodium or indazolium *cis*/*trans*-[MCl₄(1*H*-indazole)(NO)] (M = Ru, Os) complexes towards human serum albumin (HSA) and high molecular mass components of the blood serum was monitored by ultrafiltration. HSA was found to be mainly responsible for the binding of the studied ruthenium and osmium complexes. In other words, this protein can provide a depot for the compounds and can affect their biodistribution and transport processes. In order to elucidate the HSA binding sites tryptophan fluorescence quenching studies and displacement reactions with the established site markers warfarin and dansylglycine were performed. Conditional stability constants for the binding to sites I and II on HSA were computed showing that the studied ruthenium and osmium complexes are able to bind into both sites with moderately strong affinity ($\log K' = 4.4-5.1$). Site I is slightly more favored over site II for all complexes. No significant differences in the HSA binding properties were found for these metal complexes demonstrating negligible influence of the type of counter ion (sodium vs. indazolium), the metal ion center identity (Ru vs. Os) or the position of the nitrosyl group on the binding

1

event. Electron paramagnetic resonance spin labeling of HSA revealed that indazolium *trans*-[RuCl$_4$(1*H*-indazole)(NO)] and long-chain fatty acids show competitive binding to HSA. Moreover, this complex has a higher affinity for site I, but when present in excess, it is able to bind to site II as well, and displace fatty acids.

* Corresponding Authors.

E-mail addresses: ana@ffh.bg.ac.rs (A. Popović-Bijelić), enyedy@chem.u-szeged.hu (E.A. Enyedy); vladimir.arion@univie.ac.at (V.B. Arion)

1. Introduction

The compound *cis*-[PtCl$_2$(NH$_3$)$_2$] (cisplatin) is still recognized as the most prominent metal-based drug in treatment of various types of cancer and is used nowadays mostly in combination chemotherapy. Although the importance of cisplatin and the other two platinum(II)-based worldwide approved oncology drugs, carboplatin and oxaliplatin, in this area is indisputable, the observed adverse effects and sensitivity to resistance mechanisms strongly motivate the investigation of complexes of other metals, and, in particular, ruthenium, osmium, gallium, copper, iron *etc.* which exhibit marked antitumor activity, with the hope to overcome the encountered limitations [1,2]. Numerous metal complexes have been synthesized and tested as potential anticancer or antimetastatic agents. Some of them have entered phase I or II clinical trials, namely indazolium *trans*-[tetrachloridobis(1*H*-indazole)ruthenate(III)] (KP1019) [3] and its sodium salt (NKP-1339/IT-139) with an increased water solubility [4], imidazolium *trans*-[tetrachloride-dimethylsulfoxide-imidazole-ruthenate(III)] (NAMI-A) [5] or [*tris*(8-quinolinolato)gallium(III)] (KP46) [6]. While the organometallic ruthenium(II)-arene complex [Ru(η^6-*p*-cymene)Cl$_2$(pta)] (pta = 1,3,5-triaza-7-phosphatricyclo-[3.3.1.1]decane) shows anti-metastatic properties and it is a promising compound for translation to clinical evaluation [7].

Interaction of anticancer metallodrugs with proteins is of considerable interest as it might have strong influence on processes that are crucial for the biodistribution, the toxicity and the mechanism of action. Among the blood proteins, human serum albumin (HSA) is the most abundant (~630 μM) and can serve as a transport vehicle for various compounds including fatty acids (FAs), bilirubin, steroids, metal ions, and various pharmaceuticals [8]. There are seven distinct binding sites on HSA for long-chain FAs (FA1 – FA7) distributed throughout the protein in an asymmetric way [8], of which FA2, FA4, and FA5 are the highest affinity sites, as indicated by crystallographic studies [9]. The principal regions of exogenous drug binding sites are located in hydrophobic pockets in subdomains IIA and IIIA (site I and site II, respectively according to the conventional view based on Sudlow's classification) [8,10], and in the recently identified binding pocket within subdomain IB (site III) which is considered as the third major binding site [11]. Three of the seven FA binding sites overlap with the two main drug binding sites, namely FA3 and FA4 overlap with site II, and FA7 with site I [8,12]. Therefore, competition between the drugs and FAs for the same binding sites is possible, although cooperativity, or even lack of competition have been observed in some cases [13].

On the other hand, binding of a drug to HSA not merely affects the biodistribution, but can be an operative way of selective tumor targeting. Since HSA and HSA-bound drugs can accumulate in malignant and inflamed tissues such as solid tumors, due to the enhanced permeability and retention effect originated from the leaky capillaries combined with absent or defective lymphatic drainage system [14]. Therefore, interaction with albumin can be exploited for tumor targeting as well.

Detailed studies on the interaction of the ruthenium(III) complexes KP1019 and its sodium analogue (KP1339) with HSA were reported previously [15]. Both metallodrugs were found to bind into sites I and II with moderately strong affinity and this binding event is rather fast, taking place within several minutes. Data also indicated that there is no preference for either binding site, and that the counterion has only little effect on the binding event.

Ruthenium- and osmium-nitrosyl complexes with azole heterocycles were recently reported to show striking differences in their antiproliferative activity. The ruthenium compounds were found 9–18 times more active *in vitro* compared to their osmium analogues, showing IC_{50} values in the low micromolar concentration range [16]. Substitution of the non-innocent nitric oxide ligand by a carbon monoxide one was also realized in the case of ruthenium azole complexes [17]. However, ruthenium-carbonyl complexes displayed a markedly reduced antiproliferative activity *in vitro*. The observed differences and elucidation of the underlying mechanisms responsible for them have attracted our attention prompting us to investigate first their interaction with HSA.

Herein we report on the studies of the hydrolytic stability of mononitrosyl and monocarbonyl complexes *cis/trans*-[MCl₄(1*H*-indazole)(NO)]⁻ (M = Ru, Os) and *trans*-[RuCl₄(1*H*-indazole)(CO)]⁻ (Chart 1, complexes **1–6**) and the interaction of these mononitrosyl compounds with HSA by fluorescence spectroscopy and separation methods, as well as by electron paramagnetic resonance (EPR) spectroscopy using a spin labeled fatty acid (SLFA). This is an efficient and widely used method for studying the binding of FAs to albumin [18–23], as well as the competition between FAs and other compounds although its application for metal complexes is fairly rare in the literature [24]. Furthermore, displacement experiments with well-established markers for sites I and II, namely warfarin (WF) and dansylglycine (DG), respectively, were also performed and the data is discussed.

Chart 1

2. Experimental

2.1. Chemicals

Racemic WF, DG, HSA (as lyophilized powder with fatty acids, A1653 and defatted HSA used for the EPR spin labeling experiments, A3782) and serum (from human male AB plasma, H4522), 2,2'-dithiodipyridine (2,2'-DTDP), NaH_2PO_4, Na_2HPO_4, NaCl and dimethylsulfoxide (DMSO) were obtained from Sigma-Aldrich in *puriss* quality. Doubly distilled Milli-Q water was used for sample preparations. HSA solution was freshly prepared before the experiments and its concentration was estimated from its UV absorption: $\varepsilon_{280\ nm}$(HSA) = 36850 $M^{-1}cm^{-1}$ [25]. Solutions of WF and DG were prepared prior to the analyses with one equivalent of NaOH and their concentrations were calculated on the basis of their UV–visible (UV–vis) spectra: $\varepsilon_{308\ nm}$(WF) = 14475 $M^{-1}cm^{-1}$, $\varepsilon_{327\ nm}$(DG) = 5068 $M^{-1}cm^{-1}$ [15]. All samples were prepared at 25 °C in 20 mM phosphate buffer (pH 7.40) containing 0.10 M NaCl. Complexes **1**, **2**, **4**, **5** and **6** were prepared as described recently [16,17].

2.2. Synthesis of sodium trans-[RuCl₄(1H-indazole)(NO)]·2.5H₂O (3)

Indazolium *trans*-[RuCl$_4$(1*H*-indazole)(NO)] (complex **5**) [16] (100 mg, 0.20 mmol) was dissolved in water (15 mL) and stirred with preconditioned (30 min) Dowex Marathon C exchange resin (2 g) in water (20 mL) for 2 h. Then the resin was filtered off and the product was lyophilised. Yield: 80%. Anal. Calcd for $C_7H_{11}Cl_4NaN_3O_{3.5}Ru$ (M = 459.05 g/mol): C, 18.31; H, 2.42; N, 9.15. Found: C, 18.25; H, 1.98; N, 8.91. ESI-MS in MeOH (negative): m/z 391 $[RuCl_4(NO)(Hind)]^-$. ^{1}H NMR (DMSO-d$_6$, 500.26 MHz): δ 7.22 (t, 1H, J = 8 Hz), 7.51 (t, 1H, J = 8 Hz), 7.78 (d, 1H, J = 9 Hz), 7.91 (d, 1H, J = 9 Hz), 8.67 (s, 1H), 12.95 (s, 1H) ppm (Fig. S1).

2.3. Spectrophotometric and spectrofluorometric measurements

Stability of the complexes was followed using UV–vis spectrophotometry. Complexes **1−6** were dissolved in 1% (v/v) DMSO/H$_2$O at 100 µM concentration in 20 mM phosphate buffer at pH 7.40 containing 0.10 M NaCl, and followed up over 24 h. A Hewlett Packard 8452A spectrophotometer was used to record the spectra in the region of 200−800 nm using 1 cm path length at 25 °C.

Fluorescence spectra were recorded on a Hitachi-F4500 fluorometer in 1 cm quartz cell at 25 °C. All solutions were prepared in 20 mM phosphate buffer (pH 7.40) containing 0.10 M NaCl and were incubated for 2 h. Samples always contained 1 μM HSA and various HSA-to-metal complex **1−5** ratios (from 1:0 to 1:20) were used. In the site marker displacement experiments the HSA-to-site marker (WF or DG) ratio was always 1:1 and the concentration of the metal complexes was varied (from 1 to 30 equiv). The excitation wavelengths were 295, 310 or 335 nm for quenching, WF and DG displacement experiments, respectively. Emission intensities were detected in the range of 300−600 nm according to the given system using 5 nm/5 nm slit width. The conditional binding constants were calculated based on the equilibrium processes and mass-balance equations for the components detailed in the Supplementary data using PSEQUAD software [26]. Three-dimensional spectra were recorded at 210−350 nm excitation and 230-450 nm emission wavelengths.

A correction for inner filter effect and self-absorbance was necessary since fluorescence is significantly absorbed by the metal complexes at higher concentrations. The correction was carried out according to the equation (1) [27]:

$$F_{corrected} = F_{measured} \times 10^{(A(EX) + A(EM))/2} \qquad (1)$$

where $F_{corrected}$ and $F_{measured}$ are the corrected and measured fluorescence intensities, and $A(EX)$ and $A(EM)$ are the absorptivities at the excitation and emission wavelengths in the samples, respectively.

2.4. Membrane ultrafiltration−UV−vis measurements

Serum or HSA containing samples (0.50 mL) were separated by ultrafiltration through 10 kDa membrane filters (Microcon YM-10 centrifugal filter unit, Millipore) into low molecular mass (LMM) and high molecular mass (HMM) fractions by using a temperature controlled centrifuge (Sanyo, 10000/s, 5-10 min). The human blood serum was diluted 1:4 with the incubation buffer (20 mM phosphate buffer, pH 7.4, 0.1 M NaCl). In these diluted serum samples the concentration of HSA and the metal complex was ~160 μM and 80 μM, respectively. Samples contained 0, 50, 160 or 630 μM HSA and 50−320 μM metal complexes dissolved in the incubation buffer, and various HSA-to-complex ratios were applied (see Table 1). All samples

were incubated for 2 h prior to the separation at 25 °C. The LMM fractions containing the unbound metal complex were separated from HSA (or serum proteins in case of serum) and adducts [HSA–metal complex] (or [protein–metal complexes]) in the HMM fractions. The LMM fractions were diluted to 0.50 mL and the concentration of the unbound complex was determined by UV–vis spectrophotometry. The UV–vis spectra of the LMM fractions were compared with the reference spectra of the samples containing metal complex without the protein at the concentration equal to that in the ultrafiltered samples. A Hewlett Packard 8452A spectrophotometer was used to record the spectra in the region of 200–700 nm at 25 °C and a path length of 1 cm.

2.5. Interaction with Cys34 SH-group on HSA

The accessible thiol content of HSA was determined according to the 2,2'-DTDP protocol described in our previous work in details [28]. Samples containing 100 μM HSA and 5−120 μM 2,2'-DTDP in 0.10 M phosphate buffer (pH 7.00 at 25 °C) were incubated for 40 min prior to the UV–vis measurements. Thiol content of 100 μM HSA was calculated in the presence of complexes **2** or **5** (1−50 μM concentrations) in 20 mM phosphate buffer (pH 7.40) containing 0.10 M NaCl. Samples were incubated for 2.5 h at 25 °C prior to the addition of 78 μM 2,2'-DTDP, and the UV–vis spectra were recorded after 40 min.

2.6. Sample preparation for EPR measurements and EPR spectroscopy

Fatty-acid free, globulin-free HSA and 16-doxyl stearic acid (16DS) were obtained from Sigma-Aldrich. HSA was dissolved in 0.9% NaCl, pH 7.40 phosphate-buffered saline (PBS) to a final concentration of 160 μM. Complex **5** was dissolved in deionized water. The binding of the complex to HSA was examined at HSA-to-complex ratios of 1:1 and 1:6. Appropriate amounts of 10 or 25 mM ethanol stock solution of 16DS were applied to the walls of Eppendorf sample tubes and allowed to dry, as described previously [21]. A volume of 15 μL of a solution containing HSA and complex **5**, incubated for 2 h at 25 °C, was added to the sample tubes containing 16DS, gently mixed, and after 30 min drawn into 5 cm long gas-permeable Teflon tubes (Zeus industries, Raritan, NJ) for the EPR measurements. The samples used for calibration contained 80, 160, 240, 320, or 400 μM of 16DS in 0.9% NaCl, pH 7.40 PBS (Supplementary data). Ethanol stock solution of 16DS (5, 10 or 25 mM) was applied to the walls of Eppendorf sample

tubes, allowed to dry and 15 µL of 0.9% NaCl, pH 7.40 PBS was subsequently added. Three independent samples were prepared for each 16DS concentration.

The 9.5 GHz EPR spectra were recorded at room temperature on a Bruker Elexsys-II EPR spectrometer. The experimental conditions were: microwave power 10 mW, modulation amplitude 2 G, modulation frequency 100 kHz, and conversion time 240 ms. Spectra were recorded and analyzed using Bruker Xepr software.

3. Results and Discussion

3.1. Preparation of the complexes 1−6

Synthesis of complexes **1**, **2** and **4−6** was reported [16,17], while complex **3** was obtained from **5** by metathesis reaction with sodium cation exchange resin (see Experimental section). The complexes were prepared in order to investigate the effect of metal ion identity (Ru or Os), the complex configuration (*cis* or *trans*), the type of counterion (Na$^+$ or indazolium (H$_2$ind$^+$)) and the effect of the "redox active" nitrosyl and "redox inert" carbonyl ligands on the hydrolytic stability and interaction with HSA which may contribute to the understanding of the differences in their bioactivity and underlying mechanisms responsible for it.

3.2. Hydrolytic stability of the complexes 1−5

It is well known that the structural analogues of the studied ruthenium and osmium complexes, the ruthenium(III) containing KP1019 and KP1339 can undergo hydrolysis in aqueous solutions with reaction kinetics depending on the pH, concentrations of hydrogen carbonate and chloride ions in the incubation medium [29,30]. Therefore, the hydrolytic stability of the nitrosyl complexes **1−5** was checked prior to the HSA binding studies. Taking into account the concentration of chloride ions in human blood serum, our investigation was directed on the hydrolytic processes at pH 7.40 in the presence of 0.10 M NaCl. The applied concentration of the chloride ions corresponds to that of the human blood serum. The hydrolytic stability measurements for complexes **1–5** were done at 25 °C and for complexes **2** and **5** at 37 °C as well, since the actual temperature may have an influence on the hydrolysis rate. The complexes studied by UV−vis spectrophotometry were found to be stable for at least 24 h in the presence of 1% (v/v) DMSO at both temperatures (Fig. S2). The generally easily hydrolyzing chlorido ligands in the first coordination sphere of ruthenium or osmium seemed not to be exchanged by water

molecules (or hydroxides) within the given time frame. Most probably this behavior is due to the presence of the coordinated nitrosyl group, the high inertness of the metal centers, especially in case of the osmium complexes, and the hydrolysis suppressing effect of excess chloride ions present.

3.3. Hydrolytic stability of 6

Although this complex is structurally closely related to **1–5**, the exchange of the nitrosyl ligand by a carbonyl one affects dramatically its hydrolytic stability in aqueous media. In particular, the time-dependent UV−vis spectra indicate that this carbonyl compound starts to decompose in non-buffered aqueous solution (pH ~ 3.8) slowly, while the spectral changes are much faster at pH 7.40 (phosphate buffer) in the presence of 0.10 M NaCl (Fig. 1a). Absorbance changes detected at 386 nm clearly indicate the multiple nature of the hydrolytic processes, namely three different reaction steps are observed. Notably, the final spectrum resembles that of the free indazole under the employed conditions. On the other hand, parallel to these changes a significant increase of the fluorescence emission was detected (Fig. 1b). The initial intensity of the signal, which is originated from the indazolium counter ion, was increased by a factor of 2 indicating the liberation of the coordinated indazole ligand. All these findings strongly suggest the relatively fast (~30 min) decomposition of **6** in aqueous solution at physiological pH. The carbonyl ligand as strong π-acceptor compared to nitrosyl presumably has a kinetic labilizing *trans*-effect on *trans*-standing indazole ligand. The *trans*-influence of CO when compared to NO could be also observed in closely related complexes. A lengthening of *trans* Ru–N(azole) bond *trans* to Ru–CO is evident when comparing the same bond *trans* to Ru–NO. The Ru–N(indazole) bond in nBu$_4$N[*trans*-RuCl$_4$(1H-indazole)(CO)] and [(1H-indazole)H][*trans*-RuCl$_4$(1H-indazole)(CO)] is of 2.1313(13) and 2.1248(17) Å, respectively, [17] compared to 2.104(3) in H$_2$ind[*trans*-RuCl$_4$(NO)(1H-indazole)] [16]. The same trend is observed when comparing the Ru–N(azole) bond of 2.126(6) and 2.091(2) Å in (1-methylimidazole)H[*trans*-RuCl$_4$(NO)(1H-indazole)] [31] and [(1H-imidazole)$_2$H][*trans*-RuCl$_4$(NO)(1H-imidazole)] [32]. The much lower solution stability of this compound compared to that of the analogous complex **5** may be responsible for its strongly reduced antiproliferative activity. IC$_{50}$ values of 180−205 μM and 1−8 μM have been found for complexes **6** and **5**, respectively, in human cancer cell lines [16,17]. Therefore, the HSA binding studies were performed only with the nitrosyl complexes **1–5**.

9

Fig. 1.

3.4. Interaction with albumin and blood serum: ultrafiltration study

Interaction between HSA and the biologically most active complex **5** and its closely related derivatives **1−4** (Chart 1) possessing lower antiproliferative activity was studied by ultrafiltration, fluorescence and UV−vis studies. Additionally EPR spin labeling method was used in the case of complex **5**. Since the studied compounds show hydrolytic decomposition at neither 25 nor 37 °C (see section 3.2), and the conditional binding constants of the applied site marker probes towards HSA were found to be fairy similar at both temperature values in our former work [15]; here the measurements with the protein were conducted at 25 °C.

One of the most efficient approaches to investigate the direct interaction between HSA and any low molecular mass (LMM) organic molecule or metal complex is the ultrafiltration coupled with an appropriate analytical method such as UV−vis, inductively coupled plasma (ICP) mass spectrometry or ICP− atomic emission spectroscopy. This technique enables a separation of the high molecular mass (HMM) fraction (such as the protein and the protein-bound LMM compounds) from the LMM fraction containing the unbound molecules (such as the protein-free compounds). The concentration of the metal complexes in the LMM fraction was determined by UV−vis spectroscopic detection after the separation and their spectra were compared with reference spectra yielding the ratios of the unbound and total amount of the complexes. Notably, in this part of the work lyophilized HSA with fatty acids was used.

Prior to the measurements of HSA-metal complex containing adducts the compounds **1–5** without the protein were filtered in order to avoid the possible errors resulting from the retention on the filter. All *trans*-isomers **2–5** passed through the filter with 94−100% efficacy, while approximately 50% of the *cis*-configured complex **1** was stacked on the filter. Therefore, only complexes **2–5** were used to follow interactions with HSA by ultrafiltration-UV−vis, and constant HSA-to-complex ratios, namely 1:0.5 and 1:1 were used. HSA concentration was chosen at (i) 630 μM to mimic physiological conditions, (ii) 160 μM to get comparison with 4-fold diluted serum samples and (iii) 50 μM to collect data at more diluted conditions. Our preliminary UV−vis spectrophotometric measurements revealed that 2 h incubation time was enough to reach equilibrium in the HSA-complex containing samples in the given concentration range. The obtained values for the bound metal complex fractions after separation and analysis are presented

in Table 1 together with data related to KP1019 for comparison. These binding data show unambiguously that complexes **2−5** were mostly bound to HSA (92−94%) at physiological HSA concentration (630 μM). No significant differences could be observed in the binding affinity among these metal complexes to HSA. It is worth noting that the indazolium counterion was in excess in the LMM fraction after separation compared to the metal complexes in case of **4** and **5**. (Molar absorbance spectra of metal complexes and indazole were used for the deconvolution of the spectra recorded for the LMM fractions to obtain the concentrations of the unbound compounds.) This phenomenon can be explained by the weaker binding affinity of indazole, compared to the metal complex, for HSA, taking place only at site II in subdomain IIIA [15].

Table 1

At a lower (160 μM) HSA content, the bound amount of metal complexes **2−5** was slightly smaller compared to that in experiments at physiological HSA concentration (630 μM), however >80% of the complex is still bound to this serum protein. The differences between the binding affinity of the certain complexes remained within the uncertainty of the method. Further decrease in the HSA concentrations favors unambiguously the dissociation of each formed adduct. At the same time HSA at 50 μM was able to bind 64 and 70% of **5** and **2,** respectively, at 1:1 protein-to-complex ratio. Complexes **3** and **4** are still bound to HSA in outstanding 77−79% quantity. In order to obtain a general view about the possible interactions with the HMM serum components, further measurements were carried out using human blood serum. The protein bound fraction of complexes **3** and **5** displayed similar trends as found for HSA-metal complex experiments at 160 μM HSA concentration which is comparable to the presumed albumin content in 4-fold diluted serum samples. The similarity in the binding properties between the serum, and the HSA-only containing samples provides strong evidence that, among the HMM components, HSA is responsible for the majority of the binding of the studied complexes. Moreover, the considerably high albumin bound portion is comparable with the binding ability of KP1019 towards HSA (see Table 1).

3.5. Exploring possible binding sites on albumin: fluorescence and UV−vis studies

In addition to the knowledge of the overall binding level of the studied complexes to HSA, the location of the possible protein binding sites at which the interaction takes place is also an important issue. Therefore spectrofluorometric quenching and site marker displacement

techniques were used to get a deeper insight into the binding event of complexes **1–5** to HSA. Quenching experiments can give information about the binding at site I (in subdomain IIA) that is one of the two main hydrophobic binding pockets of HSA. The protein contains a single tryptophan (Trp214) which is located near site I, and is quite sensitive to changes in its environment. Following the selective excitation of Trp214 at 295 nm, the fluorescence emission intensity can be attenuated by the binding at, or in close proximity to this amino acid. The representative quenching curve (Fig. 2) demonstrates that the fluorescence intensity of Trp is remarkably decreased upon addition of **2**. It can be also seen that the curve does not tend to zero intensity. This can be explained by the weak emission of the complex alone and by the presence of other fluorophores (*e.g.* Tyr) in the protein. In case of complexes **4** and **5**, an additional extraordinary high emission occurred due to the presence of the indazolium counterion (Figs. S3, S4), while the other nitrosyl complexes are merely weakly fluorescent. The intrinsic fluorescence of the complexes was taken into account and only the spectral range over 350 nm was used for the calculations.

Fig. 2.

The measured intensities were corrected by self-absorbance and inner filter effect of the samples as well (see Experimental section). Quenching constants (logK') listed in Table 1 were computed with the aid of program PSEQUAD [26] using the whole measured emission spectra. It is seen that the calculated constants of the studied complexes are quite similar. *Cis*-isomer **1** showed a similar behavior with the *trans*-complexes **2−5**.

The displacement reactions carried out with WF at the excitation wavelength of 310 nm gave information about the binding affinity to site I of HSA, as well. The initial high fluorescence emission intensity of the [HSA–WF] adduct at the applied excitation wavelength is decreased successively upon increasing the concentration of the complexes, resulting in the non-fluorescent adduct [HSA–metal complex] and the weakly fluorescent free WF (see the representative example for the titration with complex **4** in Fig. 3).

Fig. 3.

The fit between the calculated displacement curve and the measured data is quite good (Fig. 3, inset) supporting the correctness of the calculation. The obtained displacement constants (Table 1) are in good agreement with the values obtained from the quenching experiments (*vide infra*) and correspond to moderately strong binding affinity towards site I. Another well-known

site marker DG was used to investigate the interaction on site II, the other important hydrophobic pocket of HSA using a similar approach. Calculated constants (Table 1) are slightly smaller compared to those for site I; however these values still represent a moderately strong binding at site II. Referring to the displacement constants, it is noteworthy that all the values are about one order of magnitude lower for complexes **1–5** than for KP1019. At the same time comparison of the HMM fractions obtained in the ultrafiltration study (Table 1) does not reveal such appreciable differences between the behavior of complexes **1–5** and KP1019. This observation may indicate the presence of other possible binding sites on HSA; namely partial covalent binding of complexes **1–5** to imidazole or SH moieties of His and Cys, respectively.

In order to investigate possible interactions with the single free SH-group on HSA (Cys34), 2,2'-DTDP reagent was used. Initially HSA and various amounts of the metal complexes **2** or **5,** were incubated for 2.5 h, then 2,2'-DTDP was added to the samples which reacted with the remaining free SH moiety. 2-Thiopyridone is formed in a quantitative reaction, which could be detected by UV–vis spectroscopy (see details in Ref. [28]). Our results showed no involvement of the SH group in the binding event since the same amount of free SH appeared in samples regardless of the increasing metal complex-to-SH ratios (see Fig. 4 for complex **2**). Possible nitrosylation of HSA can also be excluded due to the outstanding stability of metal-NO bond [33]. However, it can be assumed that the metal ions are not able to compete for the SH group with the reagent 2,2'-DTDP. It was found out that no irreversible interaction took place with Cys SH, which is a positive outcome, allowing for further bioavailability of the complexes. Interactions with 1-methylimidazole used as a model compound for the His-imidazole nitrogen donor atom are currently investigated in our laboratories.

Fig. 4.

3.6. Binding of complex 5 in presence of long-chain fatty acids: EPR spin labeling

Since complexes **1–5** showed similar binding affinities for HSA (Table 1), the binding of complex **5** was further studied in the presence of a stearic FA, labeled with an aminoxyl radical at position C-16 (16-doxyl stearic acid, 16DS), a spin label that has been used in many previous studies [18–20,22,23]. It is important to note that the binding of FAs to HSA is not perturbed by spin labeling of FAs [20], hence the EPR spin labeling technique can provide reliable information about the amount of the FAs bound to HSA.

The EPR spectrum of the SLFA depends on its rotational motion [21]. In solution, SLFAs tumble rapidly, almost isotropically, yielding a three narrow line spectrum that arises from the electron – ^{14}N nuclear hyperfine interaction (Fig. 5a). When the SLFA becomes immobilized by binding to HSA, its motion is severely restricted and the resulting EPR spectrum is fully anisotropic (Fig. 5b). Under the condition of incomplete binding of SLFA to HSA, due to, *e.g.* excess of SLFA, narrow lines of free SLFA will appear at positions indicated by doted lines in Fig. 5. In this case, it is possible to estimate the amount of the unbound SLFAs from the height of the high-field signal (I_{hf}) in the composite spectrum of free and bound SLFA, using a calibration curve (Fig. S5, Supplementary data). In the EPR spectrum of the SLFA-HSA complex, for the SLFA-to-protein molar ratio 6:1 (Fig. 5b) no signal of the unbound SLFA was observed, indicating that all six equivalents of 16DS can bind to HSA, as reported previously [20]. The situation is different in the case of the SLFA-to-HSA molar ratio 8:1 where the signal from the unbound SLFA can be clearly observed on the high-field side (marked with an arrow in Fig. 5c). Based on three independent measurements, and determined from I_{hf} (using Fig. S5), there is approximately one (1.1 ± 0.3) free SLFA in the buffered solution. This is consistent with the fact that there are seven FA binding sites on HSA [9] and eight SLFAs are present.

Fig. 5.

The binding of 16DS to fatty-acid free HSA (160 μM) in the presence of complex **5** is shown in Fig. 5d-f. When HSA is preincubated with complex **5,** at a 1:1 HSA-to-complex ratio, for 2 h at room temperature, and subsequently spin labeled (6:1 SLFA-to-HSA ratio), the resulting EPR spectrum (Fig. 5d) does not differ from the one shown in Fig. 5b. Namely, under these experimental conditions, the binding of complex **5** does not cause changes of the bound SLFA signal intensity or spectral width. This indicates that one equivalent of **5,** and six equivalents of SLFA, can bind concurrently to HSA. Furthermore, it may suggest that in the presence of six FAs, complex **5** binds to drug site I. Since HSA and complex **5** are present in equimolar amounts, the binding of **5** to either site I or site II might be admitted. As already mentioned, site I overlaps with one FA binding site, and site II with two FA binding sites. Given that there are a total of seven FA binding sites, and **5** can bind simultaneously with six SLFAs, it is reasonable to conclude that complex **5** binds primarily to site I. This is also in agreement with previous reports that FA7 is a low affinity FA binding site [34]. Moreover, our results from fluorescence and UV–vis measurements (Figs. 2 and 3 and Table 1) indicate that the binding of

14

all studied complexes **1−5** to site I is slightly more favored over site II. Fig. 5e shows the EPR spectrum of the bound 16DS to HSA preincubated with **5** for the molar ratio SLFA:HSA:**5** = 8:1:1. The spectrum shows a two-fold increase in line intensity of the free SLFA (I_{hf}) when compared to the spectrum in the absence of complex **5,** indicating that now there are two (2.1 ± 0.4) unbound SLFAs now. This implies that **5** was able to displace one of the seven bound SLFAs, again most probably suggesting that for the HSA-to-complex molar ratio 1:1, **5** binds to drug site I.

Next, the binding of six SLFAs to HSA was investigated in the presence of 6 equivalents of complex **5** (Fig. 5f, using SLFA:HSA:**5** = 6:1:6 ratio). The resulting EPR spectrum shows additional signals when compared to Figs. 5b and d, which arise from the free SLFA in buffer. From I_{hf} it is estimated that approximately two (1.8 ± 0.4) SLFAs are not bound to HSA. This shows that in the presence of 6 equivalents of SLFA and 6 equivalents of complex **5**, only four out of six SLFAs are bound to HSA. The reason for the two unbound SLFAs may be rationalized. First, at this HSA-to-complex ratio (1:6), **5** may bind to both drug sites I and II. Second, sites I and II overlap with three FA binding sites, which leaves only four empty FA binding sites for SLFA, hence the two free SLFAs. This indicates that there is competition between FAs and complex **5** for the same binding sites on HSA. Here, we should not exclude the possibility that under the conditions when **5** is present in excess over HSA, and in equimolar amounts as FAs, indazolium cation may bind to site II, replacing the SLFAs.

FAs are mainly transported by HSA in blood and their binding to the protein affects the interactions with other exogenous and endogenous compounds, as it was also observed in the case of complex **5**, which underlines the importance of the use of HSA in its non-fatty acid free form for the binding studies.

4. Conclusions

The main objective of this work was to characterize the aqueous solution stability of a series of [MCl$_4$(1*H*-indazole)(L)]⁻ complexes, where M = Ru or Os, L = NO or CO) and their interaction with the non-specific blood transfer protein, human serum albumin. The mononitrosyl complexes **1−5** showed unchanged UV−vis spectra when monitored over 24 h incubation period in the presence of 100 mM chloride ions and at pH 7.4 indicating their prominent hydrolytic stability. In contrast, a rapid decomposition of the monocarbonyl complex **6** takes place in

solution accompanied by the loss of the coordinated indazole ligand. Binding of antitumor metallodrugs to HSA is of considerable interest as it has a profound effect on the biodistribution in serum, and the interaction of the mononitrosyl complexes **1–5** with this protein was studied by spectrofluorometry involving Trp quenching and competition studies with well-established site markers (WF, DG), as well as by EPR spin labeling. Ultrafiltration-UV–vis method was applied to monitor the overall binding towards HSA and HMM serum components. When 630 μM of HSA was loaded with 0.5 equiv of the compounds, it was found that the protein is able to bind 92-94% of the complexes without significant effects exerted by the type of the counterion (sodium or indazolium), the metal center (Ru or Os) and the *cis*- or *trans*-configuration. The observed binding level is similar to that of the reference compound, KP1019 under similar conditions. Based on the experiments performed on the serum samples, HSA was found to be the main binding protein for the studied complexes among the serum components. The spectrofluorimetric studies indicate that the studied mononitrosyl complexes are able to bind into both sites, I and II, with moderately strong affinity, although site I is somewhat more favored. Log$K$' values of 4.9–5.1 were obtained for site I, and 4.4–4.7 for site II. According to the EPR spin labeling studies, indazolium *trans*-[RuCl$_4$(1H-indazole)(NO)] can bind to HSA in the presence of long-chain FAs, however a competition is observed between the two binders, due to the overlapping binding sites. At 1:1 HSA-to-complex ratio, the ruthenium compound **5** binds at site I in addition to the binding of up to six FAs at the same time. When **5** is present in excess over HSA, it binds to both sites, I and II, and up to four FAs can bind simultaneously.

Abbreviations

cisplatin	*cis*-[PtCl$_2$(NH$_3$)$_2$]
DG	dansylglycine
DMSO	dimethylsulfoxide
16DS	16-doxyl stearic acid
2,2'-DTDP	2,2'-dithiodipyridine
EPR	electron paramagnetic resonance
FAs	fatty acids
HMM	high molecular mass
HSA	human serum albumin

H_2ind^+	indazolium
ICP	inductively coupled plasma
KP1019	indazolium *trans*-[tetrachloridobis(1*H*-indazole)ruthenate(III)]
LMM	low molecular mass
λ_{EM}	fluorescence emission wavelength
λ_{EX}	fluorescence excitation wavelength
PBS	phosphate buffered saline
SLFA	spin labeled fatty acid
UV–vis	UV–visible
WF	warfarin

Acknowledgments

Appendix A. Supplementary data

Supplementary data to this article can be found online at …

References

[1]   Y. Jung, S.J. Lippard, Chem. Rev. 107 (2007) 1387–1407.

[2]   F. Bacher, V.B. Arion, in: Reedijk, J. (Ed.) Ruthenium Compounds as Antitumor Agents: New Developments, Elsevier Reference Module in Chemistry, Molecular Sciences and Chemical Engineering. Waltham, MA: Elsevier, 2014, doi: 10.1016/B978-0-12-409547-2.11353-8

[3]   C.G. Hartinger, M.A. Jakupec, S. Zorbas-Seifried, M. Groessl, A. Egger, W. Berger, H. Zorbas, P.J. Dyson, B.K. Keppler, Chem. Biodiversity 5 (2008) 2140–2155.

[4]   N.R. Dickson, S.F. Jones, H.A. Burris, R.K. Ramanathan, G.J. Weiss, J.R. Infante, J.C. Bendell, W. McCulloch, D.D. Von Hoff, J. Clin. Oncol. 29 (2011) 2607 (suppl., abstr.).

[5] E. Alessio, G. Mestroni, A. Bergamo, G. Sava, Curr. Top. Med. Chem. 4 (2004) 1525–1535.

[6] M.A. Jakupec, B.K. Keppler, Curr. Top. Med. Chem. 4 (2004) 1575–1583.

[7] A. Weiss, R.H. Berndsen, M. Dubois, C. Müller, R. Schibli, A.W. Griffioen, P.J. Dyson, P. Nowak-Sliwinska, Chem. Sci. 5 (2014) 4742–4748.

[8] G. Fanali, A. di Masi, V. Trezza, M. Marino, M. Fasano, P. Ascenzi, Mol. Aspects. Med. 33 (2012) 209–290.

[9] S. Curry, H. Mandelkow, P. Brick, N. Franks, Nat. Struct. Mol. Biol. 5 (1998) 827−835.

[10] X.M. He, D.C. Carter, Nature 358 (1992) 209–215.

[11] F. Zsila, Mol. Pharm. 10 (2013) 1668−1682.

[12] J.R. Simard, P.A. Zunszain, J.A. Hamilton, S.J, Curry, Mol. Biol. 361 (2006) 336−351.

[13] G. Colmenarejo, Med. Res. Rev. 23 (2003) 275–301.

[14] F. Kratz, Control. Release 132 (2008) 171–183.

[15] O. Dömötör, C.G. Hartinger, A.K. Bytzek, T. Kiss, B.K. Keppler, É.A. Enyedy, J. Biol. Inorg. Chem. 18 (2013) 9–17.

[16] G.E. Büchel, A. Gavriluta, M. Novak, S.M. Meier, M.A. Jakupec, O. Cuzan, C. Turta, J.B. Tommasino, E. Jeanneau, G. Novitchi, D. Luneau, V.B. Arion, Inorg. Chem. 52 (2013) 6273–6285.

[17] P.S. Kuhn, S.M. Meier, K.K. Jovanović, I. Sandler, L. Freitag, G. Novitchi, L. Gonzalez, S. Radulović, V.B. Arion, unpublished results

[18] J.D. Morrisett, H.J. Pownall, A.M. Gotto, J. Biol. Chem. 250 (1975) 2487−2494.

[19] T.G. Gantchev, M.B. Shopova, Biochim. Biophys. Acta 1037 (1990) 422−434.

[20] M.J.N. Junk, H.W. Spiess, D. Hinderberger, Angew. Chem. Int. Ed. 49 (2010) 8755−8759.

[21] N. Kocherginsky, H.M. Swartz, in: Nitroxide Spin Labels, CRC Press Inc., Fl. USA, 1995.

[22] A. Gurachevsky, E. Muravskaya, T. Gurachevskaya, L. Smirnova, V. Muravsky, Cancer Invest. 25 (2007) 378−383.

[23] A.A. Pavićević, A.D. Popović-Bijelić, M.D. Mojović, S.V. Šušnjar, G.G. Bačić, J. Phys. Chem. B 118 (2014) 10898−10905.

[24] H. Yuan, W.E. Antholine, W.K. Subczynski, M.A. Green, J Inorg Biochem. 61 (1996) 251–259.

[25] G.H. Beaven, S. Chen, A. D'Albis, W.B. Gratzer, Eur. J. Biochem. 42 (1974) 539–546.

[26] L. Zékány, I. Nagypál, in: D.L. Leggett (Ed.), Computational Methods for the Determination of Stability Constants, Plenum Press, New York, 1985, pp. 291–353.

[27] J.R. Lakowicz, Principles of Fluorescence Spectroscopy 3rd. Ed. Springer Science, New York, 2006.

[28] V. Pichler, J. Mayr, P. Heffeter, O. Dömötör, É.A. Enyedy, G. Hermann, D. Groza, G. Köllensperger, M. Galanski, W. Berger, B.K. Keppler, C.R. Kowol, Chem. Comm. 49 (2013) 2249–2251.

[29] T. Pieper, W. Peti, B.K. Keppler, Met. Based Drugs 7 (2000) 225–232.

[30] A. Küng, T. Pieper, R. Wissiack, E. Rosenberg, B.K. Keppler, J. Biol. Inorg. Chem. 6 (2001) 292–299.

[31] A.A. Batista, L.R.V. Olmo, C. Oliva, E.E. Castellano, O.R. Nascimento, Inorg. Chim. Acta 202 (1992) 37–41.

[32] B. Serli, E. Zangrando, E. Iengo, J. Mestroni, L. Yelowlees, E. Alessio, Inorg. Chem. 41 (2002) 4033–4043.

[33] M.J. Cleare, Platinum Metals Rev. 12 (1968) 131–133.

[34] P. Ascenzi, A. Bocedi, S. Notari, G. Fanali, R. Fesce M. Fasano, Mini Rev. Med. Chem. 4 (2006) 483–489.

Table 1

Binding affinity of complexes **1**−**5** and KP1019 for comparison to HSA (or HMM serum components); HSA-bound complex quantities (%) obtained from ultrafiltration-UV−vis studies and conditional binding constants (logK') from spectrofluorometric measurements {pH = 7.40 (20 mM phosphate buffer); 0.10 M NaCl; 25 °C}.

		1	**2**	**3**	**4**	**5**	**KP1019**
Ultrafiltration−UV−vis:				Bound complex (%)[a]			
HSA/complex (μM/μM)	630/320	-	93	92	94	92	97[b]
	160/80	-	88	92	83	81	90[b]
	50/50	-	70	79	77	64	72[b]
Serum/complex (-/μM)	-/80[c]	-	-	86	-	81	-
Spectrofluorometry:				logK'[d]			
Quenching		5.06(1)	5.10(1)	-	4.95(3)	4.92(3)	5.66[e]
WF displacement		4.98(1)	5.00(1)	-	5.00(1)	4.90(1)	5.83[e]
DG displacement		4.69(1)	4.61(1)	4.65(1)	4.58(1)	4.37(1)	5.81[e]

[a] From two parallel measurements, standard deviations: ± 3-4%.

[b] Calculated values, based on stepwise binding constants of complexes formed with HSA taken from Ref. [15].

[c] 4-Fold diluted human blood serum, c_{HSA} ≈160 μM.

[d] Standard deviations of the last given digit in parentheses.

[e] Taken from Ref. [15].

| cation	configuration	M	L	complex
Na⁺	cis	Os	NO	1
Na⁺	trans	Os	NO	2
Na⁺	trans	Ru	NO	3
H_2ind^+	trans	Os	NO	4
H_2ind^+	trans	Ru	NO	5
H_2ind^+	trans	Ru	CO	6
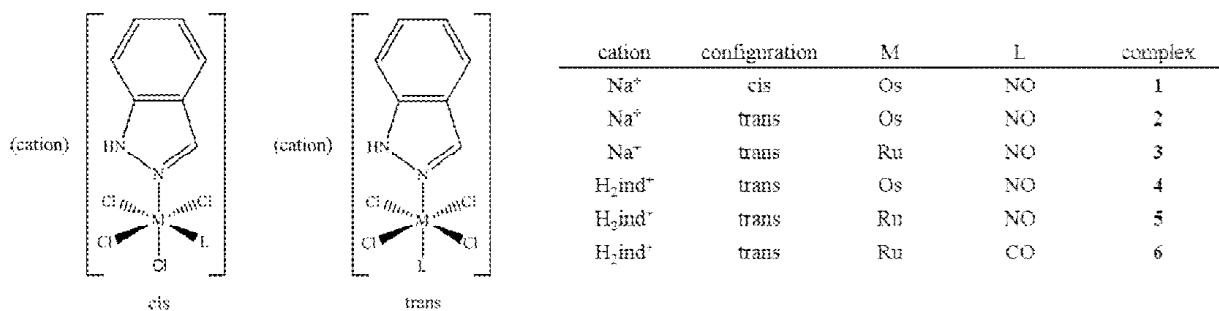
Chart 1. Complexes **1-6** studied in this work.
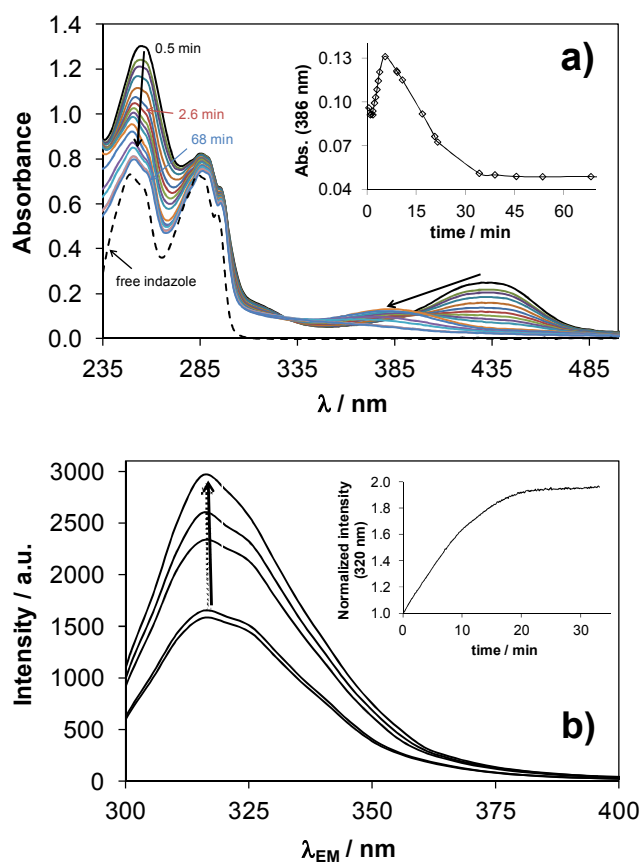
Fig. 1. Time-dependent UV−vis spectra of complex **6** {$c_{complex}$ = 80 μM, $c_{indazole}$ = 160 μM}. *Inset shows the absorbance values at 386 nm.* (a) Time-dependent fluorescence emission spectra of complex **6** {$c_{complex}$ = 6.3 μM; λ_{EX} = 290 nm}. *Inset shows the normalized (F/F₀) intensities at 320 nm.* (b). {pH 7.40 (20 mM phosphate buffer); 0.1 M NaCl; 25 °C}.

21
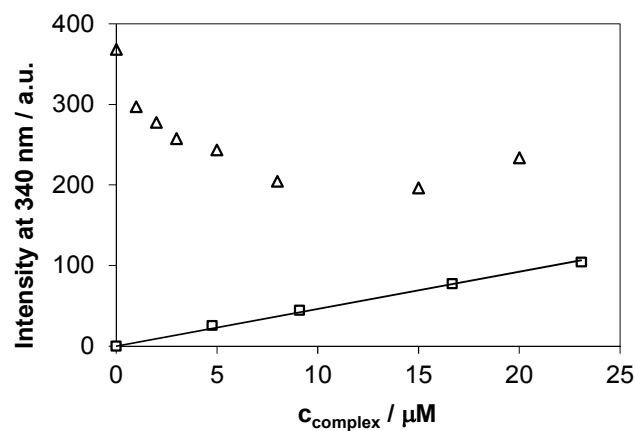
Fig. 2. Quenching of Trp fluorescence of HSA by the addition of complex **2** (Δ) and calibration curve for the metal complex alone ($\square$) {c_{HSA} = 1 μM; λ_{EX} = 295 nm; λ_{EM} = 340 nm; pH = 7.40 (20 mM phosphate buffer); 0.1 M NaCl; 25 °C}.
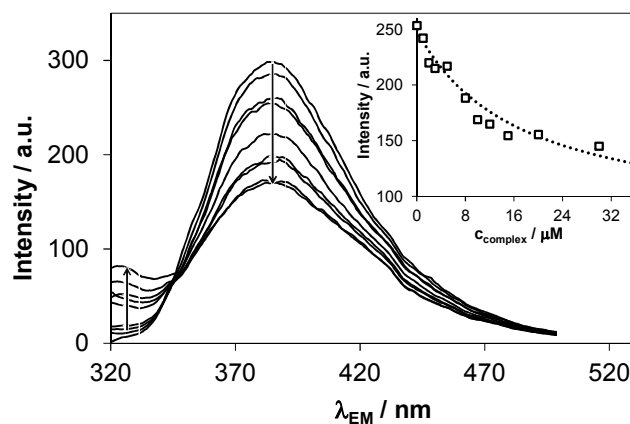
Fig. 3. Fluorescence emission spectra obtained upon the titration of HSA–WF (1:1) with complex **4** {c_{HSA} = c_{WF} = 1 μM; $c_{complex}$ = 0–30 μM; λ_{EX} = 310 nm; pH = 7.40 (20 mM phosphate buffer); 0.1 M NaCl; 25 °C}. *The inset shows the concurrence of the measured (squares) and the calculated (dotted line) intensities at 400 nm for various complex total concentrations.*
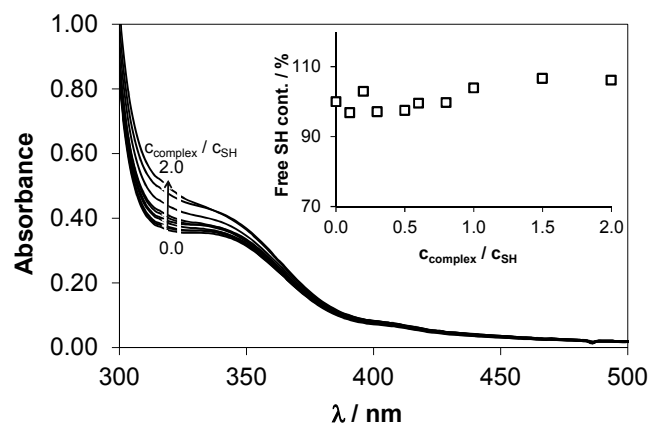
Fig. 4. Detection of free SH content in HSA – complex **2.** Absorbance spectra of 2-thiopyridone for increasing c(metal complex) / c(SH) ratios. {c_{HSA} = 100 μM from this accessible thiol groups: c_{SH} = 25.0 μM; $c_{complex\ 2}$ = 0–50 μM; $c_{2,2'\text{-DTDP}}$ = 78.0 μM; pH = 7.40 (20 mM phosphate buffer); 0.10 M NaCl; 25 °C}. *Inset shows the free SH content of HSA at various metal complex-to-HSA ratios after 2.5 h incubation period.*
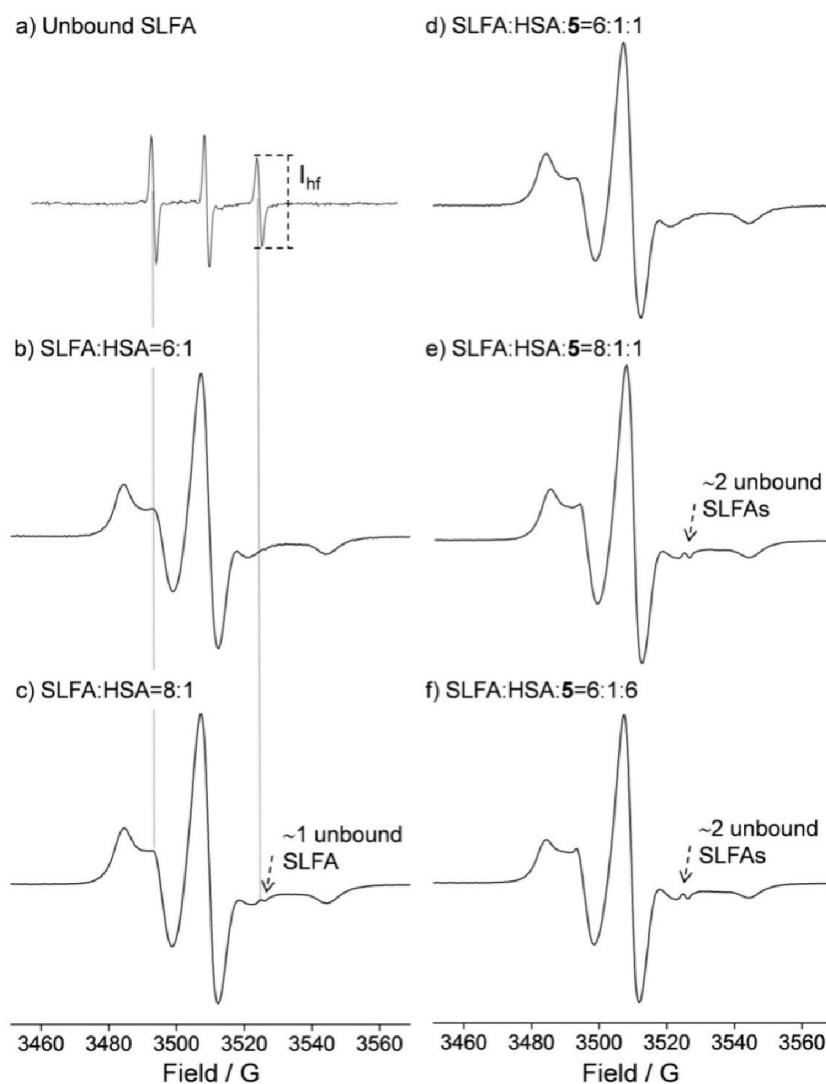
Fig. 5. Free (unbound) 160 μM 16DS in PBS buffer (a). EPR spectra of 16DS bound to HSA in the absence (b and c), and in the presence (d, e and f) of complex **5**, for the SLFA:HSA molar ratios 6:1 (b, d and f), and 8:1 (c and e). All samples (except a) contained 160 μM HSA in PBS. Samples d and e contained 160 μM complex **5**, and sample f contained 960 μM complex **5**. The intensity of the high-field peak in the spectrum of the unbound 16DS (a) is marked as I_{hf}.
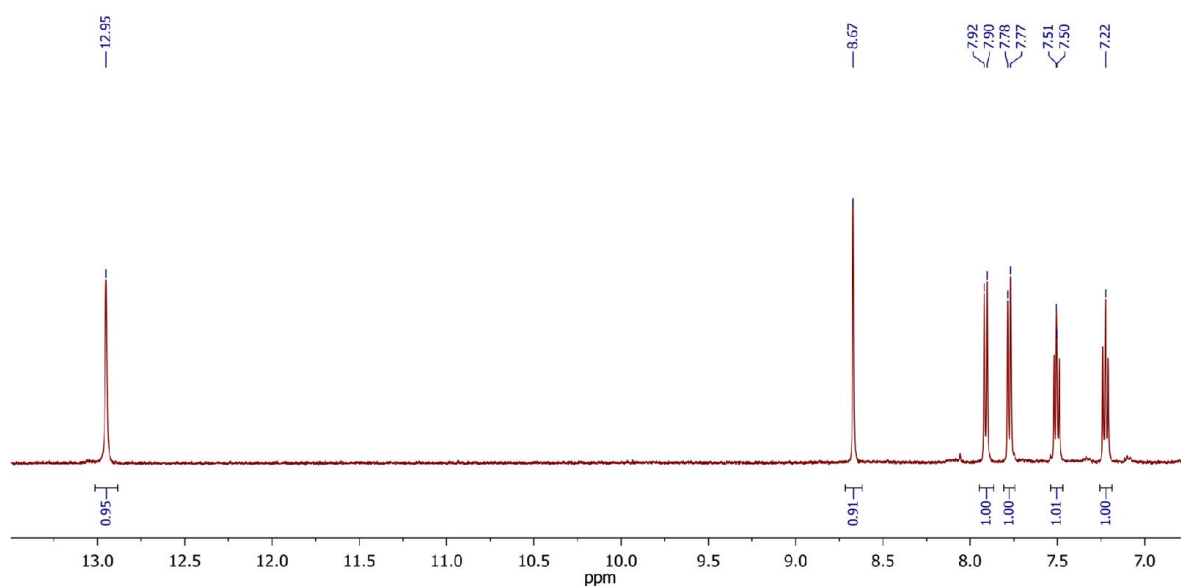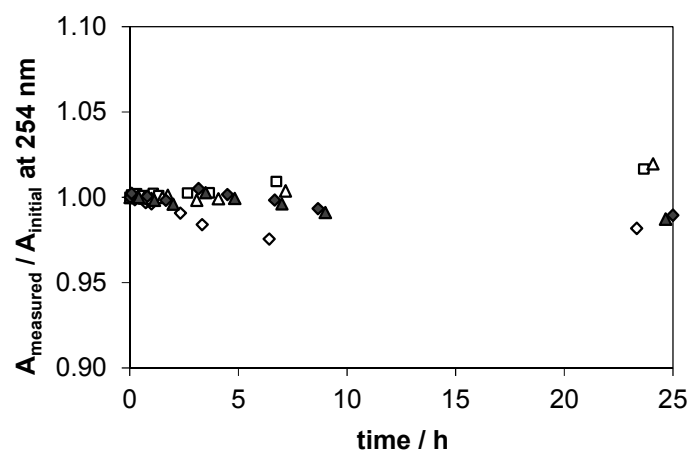
SUPPLEMENTARY DATA

Investigation of the binding of *cis/trans*-[MCl₄(1*H*-indazole)(NO)]⁻ (M = Ru, Os) complexes to human serum albumin

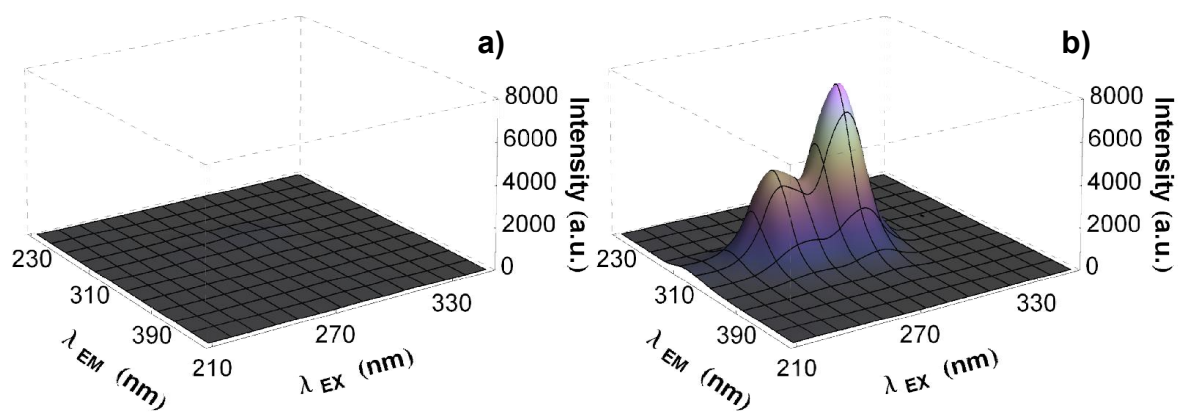*O. Dömötör, A. Rathgeb, P.S. Kuhn, A. Popović-Bijelić, G. Bačić, E. Anna Enyedy, V.B. Arion*

Figure S1. ^{1}H NMR spectrum of complex **3** in DMSO-d_6.

Fig. S2. Time-dependence of absorbance values at 254 nm of complex 2 (Δ, $\blacktriangle$), 4 ($\square$), and 5 ($\Diamond$, $\blacklozenge$) measured at 25 °C (empty markers) and at 37 °C (filled markers) {c_{complex} = 100 µM; pH = 7.40 (20 mM phosphate buffer); 0.1 M NaCl; 1%(v/v) DMSO}

**Fig. S3.** The 3-dimensional fluorescence spectra of complex **2** (a) and **4** (b) {c_{complex} = 10 µM; pH 7.40 (phosphate buffer); 0.1 M NaCl; 25 °C}
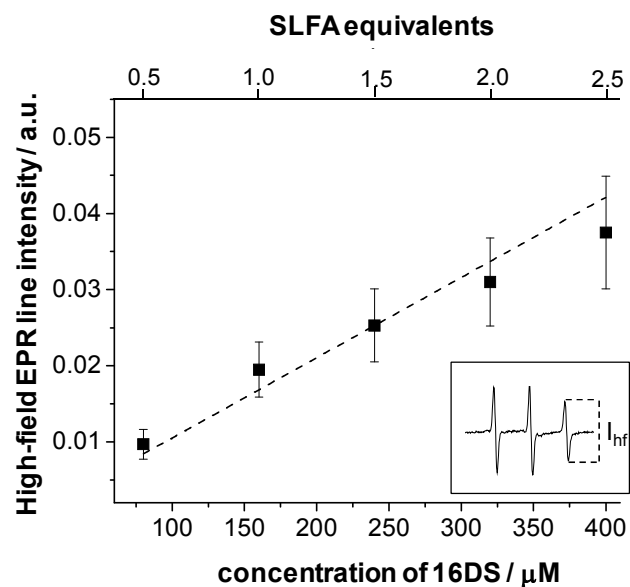
Fig. S4. The high-field EPR line intensity dependence on the concentration of 16DS. Three independent samples were prepared for each 16DS concentration. The bottom abscissa shows the actual concentration of 16DS in the samples. The top abscissa shows the number of the unbound SLFA equivalents that correspond to the samples that contain 160 μM HSA. A typical EPR spectrum of free 16DS in PBS buffer is shown in the inset. The intensity of the high-field EPR line is marked as I_{hf}.

Determination of conditional binding constants (K') for HSA-ligand adducts from the spectrofluorometric quenching or site marker displacement measurements:

Calculations are based on the general *chemical equilibrium* (number of components is 2: ligand and HSA), where ligand = complex **1-5** or site marker (WF, DG):

$$p \,(\text{ligand}) + q \,(\text{HSA}) \rightleftharpoons (\text{ligand})_p(\text{HSA})_q$$
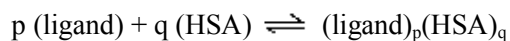
$$K_{pq}' = [(\text{ligand})_p(\text{HSA})_q] \,/\, ([\text{ligand}]^p \times [\text{HSA}]^q);$$

and *mass balance equations* for the components:

$$c_{ligand} = [\text{ligand}] + \sum_{i=1}^{n} p_i\, K'_{pq}[\text{ligand}]^{p_i}[\text{HSA}]^{q_i} \;;\; c_{HSA} = [\text{HSA}] + \sum_{i=1}^{n} q_i\, K'_{pq}[\text{ligand}]^{p_i}[\text{HSA}]^{q_i}$$

where,
K_{pq}' = conditional binding constant of the HSA-ligand adducts
c_x = analytical (total) concentration of component x
$[x]$ = equilibrium concentration of component x
q, p = 1 assumed under the conditions of fluorometric studies due to the highly diluted samples

whereas,

$$I_i = \phi_{ligand}^{i} \times [\text{ligand}] + \phi_{HSA}^{i} \times [\text{HSA}] + \phi_{HSA-ligand}^{i} \times [\text{HSA - ligand}]$$

where,
I_i = fluorescence emission intensity at "i" nm
ϕ_x^i = proportional constant for component x at "i" nm (between I^i and equilibrium concentration of x); "molar intensity"
Strictly identical parameters of the instrument are used at each measuring set.

The equation system was solved with a non-linear least squares method via iterative cycles by the program PSEQUAD [*L. Zékány, I. Nagypál, in: Computational Methods for the Determination of Stability Constants (Ed.: D. L. Leggett), Plenum Press, New York, 1985, pp. 291–353.*].

The indazolium counter cation in the complexes **4** and **5** has intrinsic emission when excited at 295 nm which cannot be neglected in the Trp-quenching studies when the binding event at site I is monitored. Indazole shows no binding at site I (only a weak binding at site II) based on site marker probe experiments [*O. Dömötör, C.G. Hartinger, A.K. Bytzek, T. Kiss, B.K. Keppler, E.A. Enyedy, J. Biol. Inorg. Chem. 18 (2013) 9–17.*]. On the other hand the intrinsic emission of indazole is not sensitive to the binding to HSA, thus it is unchanged upon the binding. That is why the contribution of the indazolium cation to the measured emission intensity is constant in the Trp-quenching experiments. Thus the emission intensity of the indazolium cation was calculated according to its actual concentration in the samples using an external calibration and was deducted from the measured emission intensities.

In the HSA-site marker systems the site marker and its protein adduct emit; the fluorescence of the protein alone is negligible under the conditions used. The obtained constants for the HSA-site marker adducts are in reasonably good agreement with our previously published data (logK' HSA-WF = 5.58 and logK' HSA-DG = 5.24 [*O. Dömötör, C.G. Hartinger, A.K. Bytzek, T. Kiss, B.K. Keppler, E.A. Enyedy, J. Biol. Inorg. Chem. 18 (2013) 9–17.*])
In the case of the site marker displacement experiments the number of components is 3 (HSA, the metal complex and site marker), thus the number of the chemical equilibria for the formation of the adducts and

the mass balance equations is increased. During the calculations of the site marker displacement constants, the constants of the HSA-site marker adducts obtained from the independent titrations were kept constant.

EPR spin labeling: The method to determine the amount of the unbound SLFAs to HSA

The amount of the unbound spin labeled fatty acids (SLFAs) in the EPR spectra of 16-doxyl stearic acid (16DS) bound to HSA in the absence/presence of indazolium *trans*-[RuCl$_4$(1*H*-indazole)(NO)] (complex **5**), was determined using a calibration curve (Fig. S4). The calibration samples contained 80, 160, 240, 320, and 400 μM 16DS in 0.9% NaCl, pH 7.40 PBS. Higher 16DS concentrations should not be used as pronounced formation of micelles is observed in the EPR spectra (see for more details on analysis of the EPR spectra of SLFA bound to HSA: *A.A. Pavićević, A.D. Popović-Bijelić, M.D. Mojović, S.V. Šušnjar, G.G. Bačić, J. Phys. Chem. B 118 (2014) 10898–10905*). These concentrations were selected with respect to the final HSA concentration (160 μM) in the samples that were used for the study of the binding of 16DS to the protein to give to the following SLFA-to-HSA molar ratios: 0.5, 1.0, 1.5, 2.0, and 2.5. The acquired EPR spectra were normalized and the height (intensity) of the high-field signal (I_{hf}) was measured.

The calibration curve is used to determine the concentration of the unbound SLFAs in the EPR spectra of 16DS bound to HSA in the absence/presence of complex **5**. The high-field peak in the EPR spectrum of the unbound 16DS in PBS (Fig. 5a) has the same line−width as that in the spectrum of 16DS in complex with HSA in PBS (Fig. 5c), as well as in the spectra of 16DS bound to HSA in the presence of complex **5** (Figs. 5e and 5f). Therefore, it is possible to compare their I_{hf} values and to determine the concentration of the unbound 16DS in the EPR spectra of 16DS/HSA/(complex **5**), (Figs. 5c, 5e, 5f), using the calibration curve shown in Fig. S3. Of note, the values of I_{hf} are not used for spin quantification but only to be compared with other intensities. Finally, the determined concentrations of the unbound 16DS were correlated to the number of SLFA equivalents that are unbound to exactly 160 μM HSA. The results are expressed as the mean value of the number of unbound SLFA equivalents determined from three independent measurements ± the standard deviation.